Article

pubs.acs.org/Biomac

Vertically Aligned Peptide Nanostructures Using Plasma-Enhanced Chemical Vapor Deposition

Milana C. Vasudev,[†] Hilmar Koerner,[†] Kristi M. Singh,[†] Benjamin P. Partlow,[‡] David L. Kaplan,[‡] Ehud Gazit,[§] Timothy J. Bunning,[†] and Rajesh R. Naik*,[†]

[†]Soft Matter Materials Branch, Materials and Manufacturing Directorate, Wright-Patterson Air Force Base, Dayton, Ohio 45433, United States

[‡]Department of Biomedical Engineering, Tufts University, Medford, Massachusetts 02155, United States

[§]Molecular Biology and Biotechnology Department, Tel Aviv University, Tel Aviv 69978, Israel

Supporting Information

ABSTRACT: In this study, we utilize plasma-enhanced chemical vapor deposition (PECVD) for the deposition of nanostructures composed of diphenylalanine. PECVD is a solvent-free approach and allows sublimation of the peptide to form dense, uniform arrays of peptide nanostructures on a variety of substrates. The PECVD deposited D-diphenylalanine nanostructures have a range of chemical and physical properties depending on the specific discharge parameters used during the deposition process.

INTRODUCTION

Plasma-enhanced chemical vapor deposition (PECVD) is a form of chemical vapor deposition where inert gas plasma is used to enhance reactivity of organic/inorganic chemical species for the deposition of thin films. Plasma polymerization for thin film coatings is a well-established method, and has generally been used in the deposition of inorganic materials and metals with high vapor pressures.[1−4] Recently, PECVD has been used in the deposition of organic films of materials such as hexafluorobenzene, hexamethyldisiloxane for biomedical, optical and telecommunication applications.[5−7] Of particular interest is the use of PECVD for the deposition of unconventional, organic, multilayer thin films for photonic applications such as notch filters and antireflective coatings.[8] The use of plasma ionization allows a dry deposition technique for the formation of stable, pinhole-free thin films which makes it an attractive alternative to conventional methods such as spin-coating, spin-assisted layer-by-layer (LbL) assembly or Langmuir−Blodgett films.[9] The plasma used in the PECVD process allows control over the composition of the processed films imparting unique surface properties without modifying the bulk material properties of the substrate. PECVD has also been used in nanostructure fabrication, thin film deposition and chemical modification of surfaces.[10,11] This state-of-the-art process can be extended to the deposition of solid monomers by adding the sublimation capability. Most biological monomers of interest exist in solid state and the capability of sublimation in the PECVD processing allows deposition of nanostructured thin films composed of these monomers. Single amino acids or simple peptides, which are structurally similar to chemical monomers, can be deposited via low pressure PECVD and the deposition of ultrathin, conformal coatings of single amino acids on substrates with varying topography has been demonstrated recently.[12,13]

Short peptide sequences have the ability to self-assemble into nanostructures when crystallized either from aqueous or nonaqueous solutions. Gazit et al. first observed the formation of peptide nanotubes while studying the formation of amyloid fibrils from aromatic peptides and identified diphenylalanine as the key recognition element in the β-amyloid peptide.[14] There have been several reports of the deposition of peptide nanotubes composed of diphenylalanine both in aqueous and organic solutions as well as via physical vapor deposition.[14−20] The self-assembly process in solution was initiated by fast solvent-evaporation at high peptide concentrations.[14,15] Physical vapor deposition of the peptide nanotubes has also been investigated to potentially avoid the use of solvents and complicated chemical synthesis routes.[18,19] Such self-assembled peptide nanostructures were found to possess unique optical, mechanical and electrochemical properties.[21−24] The self-assembly of the dipeptides is attributed to the $\pi-\pi$ stacking interaction between the π-electrons in the aromatic ring,

Received: October 5, 2013
Revised: December 13, 2013
Published: January 8, 2014

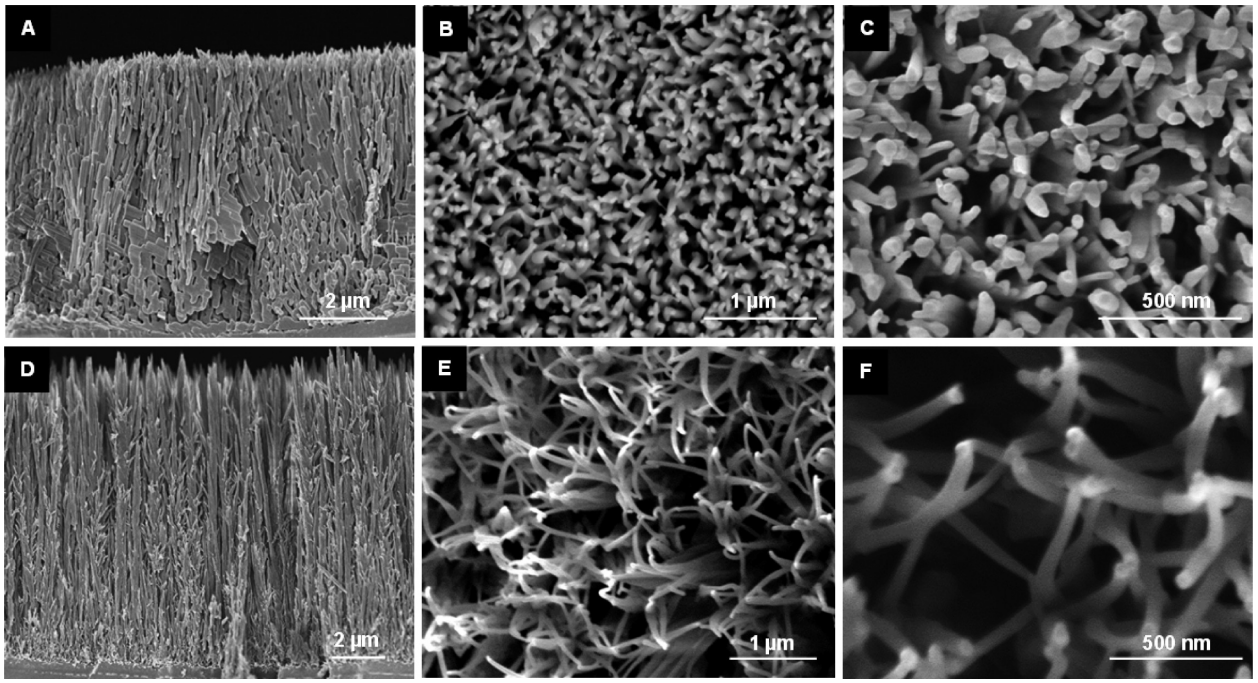

Figure 1. SEM images of vertical arrays of D-diphenylalanine nanotubes obtained using a modified PVD process in the absence of plasma (A−C) and PECVD (D−F) under pulsed conditions with RF power (30 W), frequency (100 Hz), and duty cycle (25%). (A,D) Cross-sectional views; (B,C,E,F) Top view of nanotubes.

hydrogen bonds, and hydrophobic interactions. There are several factors such as concentration of the dipeptides, temperature, and pH of the solvents which influences the formation of these nanotubes. A recent study using molecular dynamics simulations shows that aromatic interactions is the driving force for self-assembly of these dipeptide structures and is dependent on the peptide−peptide and peptide-water interactions as well as the concentration.[25] In this study, we have demonstrated the sublimation of diphenylalanine peptide into a plasma zone and subsequent deposition of vertically aligned nanotubes on a substrate using plasma-enhanced chemical vapor deposition (PECVD). The adaptation of PECVD for the deposition of peptides offers a robust, alternate method to create peptide nanostructures without the need for solvents.

EXPERIMENTAL SECTION

Materials. L-diphenylalanine and D-diphenylalanine were purchased from Bachem (Bubendorf, Switzerland). The compound 1,1,1, 3,3,3-hexafluoro-2-propanol (HFIP) was purchased from Sigma.

Synthesis of peptide nanotubes. Peptide nanotubes were deposited using a solution based method modified from Reches et al., by dissolving the lyophilized form of the peptides in HFIP followed by dilution in water.[15] The nanotubes were deposited on silicon substrates and subsequently used for comparison with the PECVD samples (Supporting Information Figure S1). A custom built plasma chamber was used for PECVD deposition of diphenylalanine by direct sublimation of the solid monomer into the plasma stream, the chamber construction is described elsewhere.[26] Silicon wafers, PDMS, graphene, and silk films were used as substrates for the deposition of peptide nanotubes. The PECVD process uses radio frequency (RF) plasma at 13.56 MHz to induce radicalization of diphenylalanine monomer species in the reaction chamber. The power supply used for the plasma generation consists of a radio frequency generator and a matching box in order to minimize reflected power. The plasma chamber was modified to support a ConFlat flange with two high current copper feed-through mounted at the bottom of the glass reactor. The modified system has a 46 mm deep tantalum heating boat (Kurt J. Lesker Co) for the sublimation, which is approximately 6 cm below the substrate. The tantalum boat was loaded with a small amount of the monomer (8−10 mg), sublimed at ∼200 °C while the substrate was maintained at room temperature downstream from the plasma zone to avoid plasma bombardment effects. Deposition was carried out under low vacuum conditions with a chamber pressure of 0.05 Torr and argon gas (99.99% purity) at a flow rate of 10 cm^3/min. Other deposition conditions such as RF power, pulsing frequency and duty cycle were varied. The RF power mode was switched between continuous and pulsed mode with frequency ranging between 100 Hz to 2 kHz and the duty cycles was constant at 25%. Power for all the depositions was kept constant at 30 W. The power supply also includes a pulse generator for power modulation where the duty cycle is the fraction of the total time the power was applied [DC = T_{on}/(T_{on} + T_{off})]. Because of the constant power and duty cycle applied during the deposition process, the average power for all the depositions can be calculated to be 7.5 W using standard RF power equations. The combination of low plasma power and low duty cycle during the deposition process helps the activation as well as the retention of chemical activity of the deposited molecule.[2,27,28]

Electron Microscopy. SEM images were obtained on Hitachi S5200 UHR field-emission scanning electron microscope (FESEM) with an accelerating voltage of 2 kV. The samples were coated with 50−70 Å of tungsten or gold. The morphology of the peptide nanotubes was determined as a function of various deposition conditions (power, frequency,

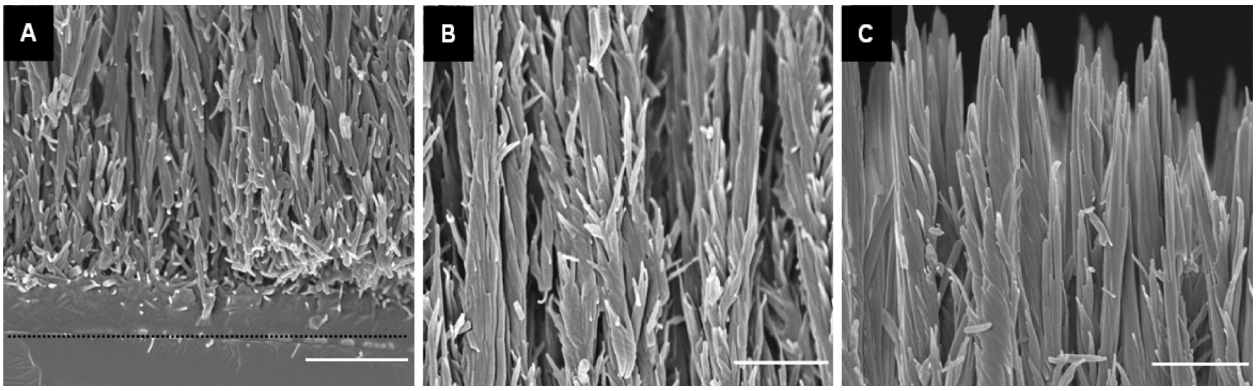

Figure 2. Cross-sectional SEM images of (A) proximal and (B−C) distal regions of vertical arrays of D-diphenylalanine nanostructures obtained using PECVD using pulsed conditions with RF power (30 W), frequency (100 Hz) and duty cycle (25%) indicating the bulk-surface heterogeneity. Dashed line denotes the interface between the silicon substrate and basal peptide seed layer. Scale bar is 500 nm for all images.

argon flow-rate, and deposition time) and both surface and cross-section images were obtained.

Fourier-Transform Infrared (FTIR) and Circular Dichroism (CD) Spectroscopy. Infrared spectra were obtained by using a Nicolet Nexus 470 FTIR spectrometer fitted with a helium neon laser and the transmission values were determined using the OMNIC program. Fourier self-deconvolution (FSD) of the infrared spectra in the amide I region was performed according to previously published procedures. Measurements were made with 4 cm^{-1} resolution. CD measurements were performed to estimate the secondary structure using a JASCO J-810 spectropolarimeter. The peptide nanotubes were removed from the silicon substrate by sonication in water. A quartz cell of path length 1 mm was used in all the measurements. Spectra were collected over the wavelength range 300−180 nm at 25 °C and background corrected using a solvent blank solution.

X-ray Diffraction Measurements. Synchrotron X-ray experiments were conducted at beamline 7.3.3 at the Advanced Light Source at Livermore Berkeley National Laboratory at 10 keV (1.24 Å) from a bend magnet and focused via a Mo/B4C double multilayer monochromator. A Dectris Pilatus 1 M detector was used to collect 2D WAX patterns at sample-to-detector distances of 1.5 m. The 2D images were reduced using the Nika data reduction package for Igor Pro. The 1D WAX experiments in in-plane and grazing geometry (out-of-plane) were carried out with a Rigaku Smartlab using CuKα radiation.

Mechanical Property Measurements. The Nanoindenter XP instrument by Agilent with a continuous stiffness measurement (CSM) option was used in order to measure the bulk Young's modulus of the peptide arrays on a silicon substrate. A cylindrical flat-punch indenter (40 μm tip) was used in the measurement of contact force. In situ SEM compression was performed using a custom-built micromechanical test frame within an FEI Quanta ESEM. Compression utilized a 40 μm × 40 μm diamond flat punch. Displacement data was acquired using the National Instruments Labview program.[29]

RESULTS AND DISCUSSION

Vapor phase deposition of the peptide nanotubes can potentially avoid the use of harsh chemicals such as HFIP, which is generally used for solvent-based synthesis of peptide nanotubes. The D-diphenylalanine monomer was heated to about ∼200 °C and sublimed into the plasma stream. This resulted in the deposition of conformal films on the substrates downstream of the plasma. Observation of the deposited D-diphenylalanine films using SEM analysis indicated the presence of large arrays of vertically aligned peptide nanotubes with open ends at the nanotube tips (Figure 1). The deposited nanotubes exhibited high aspect ratios with the length in the range of tens of micrometers and diameters of 50−300 nm. PECVD deposition of polymeric films of organic molecules such as D-diphenylalanine have a whole spectrum of chemical and physical properties depending on the specific discharge parameters used during the deposition process such as input power, chamber pressure, flow rate of the argon gas, and substrate position. The other main factor is the number and lifetime of the plasma species such as ions, radicals, and metastables formed during the reaction. This particularly offers scope of compositional and microstructural tuning of the polymeric films.[4,30] The monomer, D-diphenylalanine upon sublimation in the tantalum boat rises into the plasma stream where the monomer undergoes ionization and free radicals are also formed in the plasma. At the substrate surface, the monomer undergoes polymerization and forms a basal seed layer from which the multibranched structures of nanotubes grow. The use of pulsed plasma allows retention of the original chemistry of the monomer and allows conventional polymerization to occur during the plasma "off" time and maybe more suitable for biological monomers.[2,4,7,9,30]

For comparison, peptide nanotubes were also grown in a modified physical vapor deposition (PVD) process, by sublimation of diphenylalanine in the PECVD chamber in the absence of the plasma.[18] The nanostructures formed using PVD appear to be morphologically different when compared to the PECVD deposited nanostructures (Figure 1). The dipeptide arrays deposited by PVD appear less organized and the tips of the nanotubes are closed. In cross-sectional views (Figure 1D), the proximal ends of the PECVD deposited dipeptide nanotube arrays appear to be more homogeneous, while the PVD deposited structures are discontinuous (Figure 1A). Higher-magnification images of the distal ends of the peptide arrays show clear differences in the morphology of peptide nanotubes. The PECVD deposited D-diphenylalanine nanostructures have more of a tube-like morphology compared to the PVD grown dipeptide nanostructures (Figure 1F). The ends of the PECVD nanotubes are uniform and possess a high volume fraction of open tubes. The fibrils are usually hollow and sub-100 nm in diameter. Unlike physical vapor deposition (PVD), the

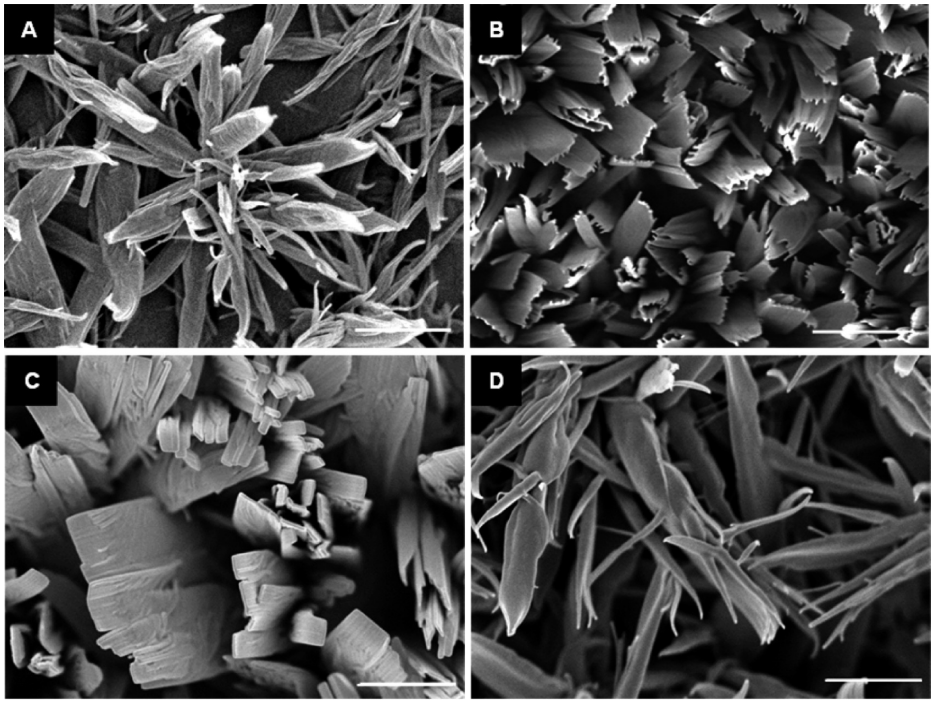

Figure 3. SEM images (top view) of D-diphenylalanine nanostructures grown under different deposition conditions with constant RF power of 30 W and 25% duty cycle pulsed PECVD at (A) 250 Hz; (B) 500 Hz; (C) 750 Hz; and (D) continuous PECVD. Scale bar is 1 μm for all images.

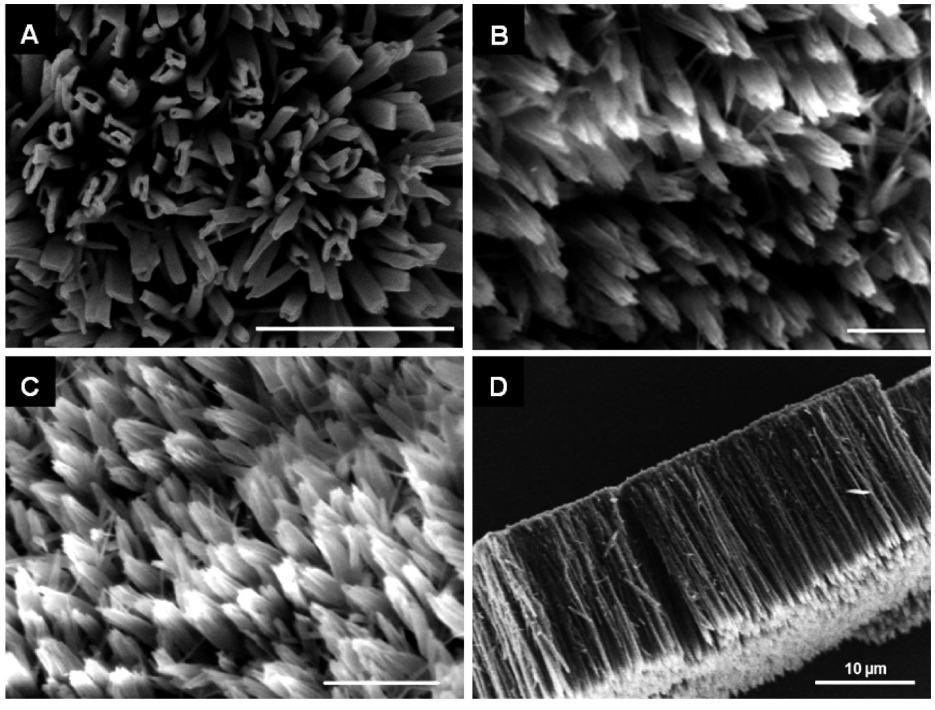

Figure 4. Demonstration of the deposition of diphenylalanine nanotubes on various substrates. SEM images of PECVD-deposited diphenylalanine nanostructures on (A) carbon electrode; (B) graphene sheet; (C) PDMS; (D) PECVD grown nanotubes detached en bloc from the PDMS substrate. In all cases, PECVD pulsed conditions with RF power (30 W), frequency (100 Hz) and duty cycle (25%). Scale bar in images (A–C) is 1 μm.

morphology and density of the nanotubes can be controlled by varying the PECVD conditions. The peptide nanotubes deposited by PECVD show structural variation along its length. Closer examination of the proximal and distal ends of the peptide arrays are shown in Figure 2. At the proximal end, peptide nanotube branches, originating from the basal seed layer, form bundles composed of the individual nanotube fibers. At the distal end, the bundles begin to flare out into fibrils, narrowing to ~50 nm in diameter. Both L- and D-isomers of diphenylalanine, and other dipeptides such as dityrosine and phenylalanine-tyrosine produced vertically aligned peptide

nanostructures using PECVD (Supporting Information Figure S2).

As mentioned earlier, the morphology and density of the nanotubes can be easily controlled by varying the conditions for PECVD. Figure 3 shows the differences in morphologies in the diphenylalanine nanotubes grown on a silicon wafer under varying deposition conditions starting with the continuous plasma to pulsed plasma depositions with constant duty cycle with increasing frequency. Changing frequency or the pulse duration is the main contributor to the differing morphologies. These parameters control the degree of plasma ionization that in turn influences the morphology and chemical composition of the deposited material. With changing frequency and duty cycle, we have observed changes in the gross morphology of the deposited nanostructures from nanotubes to nanoribbon-like structures. Average input power is controlled by changing the peak power with a continuous wave discharge or by using a pulsed wave discharge where the duty cycle dictates the amount of time that the peak power is applied. At higher frequencies, ribbon-like structures appear with larger widths at the higher frequencies (Figure 3A−C). Unlike pulsed plasma deposition, the continuous plasma deposition resulted in disordered structures with a mixture of both ribbon-like and fibrillar structures (Figure 3D). By controlling power, frequency and duty cycle, we were able to reproducibly deposit arrays of open tubular nanostructures with diameters of 50−100 nm at the distal ends, while higher frequencies and duty cycles ribbon-like nanostructures were formed. Such morphological changes have not been observed in the peptide nanotubes grown in solution-phase. The vertically aligned forests of D-diphenylalanine nanotubes showed RMS roughness on the order of 600 nm per 50 μm scan due to height discrepancies as measured on an Asylum MFP-3D AFM (Supporting Information Figure S3). Detached nanotubes grown via pulsed PECVD were deposited on a prefabricated electrode substrates and probed in the electrostatic force measurement (EFM) mode on the Asylum MFP-3D AFM to demonstrate that the nanotubes had hollow interiors[31] (Supporting Information Figure S4). The peptide nanostructures produced by PECVD typically possess high aspect ratios, where the length of the nanotubes can be easily controlled by varying the PECVD deposition conditions and surfaces coated with diphenylalanine nanotubes are hydrophobic (Supporting Information Figure S5). The PECVD deposited nanostructures were found to be at least twice the length of the PVD deposited nanotubes grown for the same duration of time.

PECVD also allows for the formation of uniform and homogeneous forests of nanotubes on a variety of substrates used in the deposition process. In Figure 4, SEM images of the diphenylalanine nanotubes obtained on the surface of carbon electrode, graphene, and elastomer (PDMS) are shown. The open ended tubes can be clearly observed when a carbon electrode substrate was used for deposition (Figure 4A). The dipeptide nanotube arrays on graphene and PDMS appeared similar to each other but differed from the nanotubes on the carbon electrode surface, exhibiting polygonal structures. Currently, we have no explanation for this observation, and detailed studies of the effects of the growth process on the substrates will be needed to address this. Interestingly, the intact vertically aligned nanotube arrays can be easily detached from the PDMS surface (Figure 4D). These examples demonstrate the ease of PECVD use for deposition on a variety of substrates.

The mechanism of self-assembly of the biomolecules in liquid environments has been studied in the past and involves hydrogen bonding and $\pi-\pi$ stacking interactions but the mechanism of peptide nanotube formation via vapor deposition has not been established. The use of elevated temperatures in the sublimation process may lead to thermally induced chemical changes in the peptide structures. MALDI-TOF analysis was used to verify that the diphenylalanine monomers undergo cyclization upon sublimation during the PECVD process (Supporting Information Figure S6). The cyclization of diphenylalanine has been seen in other methods used in the formation of diphenylalanine peptide nanotubes.[18] We further characterized these nanostructures using a variety of techniques including FTIR, CD spectroscopy, and X-ray diffraction to gain insight into the secondary structures formed by the PECVD deposited dipeptides compared to PVD grown nanotubes. As mentioned earlier, MALDI-TOF mass spectroscopy revealed cyclization of PECVD-deposited diphenylalanine, similar to observations seen with HFIP or PVD grown nanotubes. FTIR analysis of the diphenylalanine nanotubes gives us an insight into their secondary structure. The PECVD grown peptide nanotubes show peaks in the amide I region (1650−1700 cm^{-1} range), indicating β-sheet conformation.[14,32] We used Fourier self-deconvolution of the infrared spectra in the amide I region to evaluate the secondary component of the diphenylalanine nanotubes deposited using PVD or PECVD (Figure 5).[33] The structural information based on the spectrum deconvolution within the amide I region indicates an increase in the β-sheet content of PECVD deposited nanotubes when compared to the PVD (Supporting Information Table S1). This could be attributed to more ordered morphologies due to stacking of the aromatic rings and increased hydrogen bonding during the PECVD process compared to PVD process.

CD spectral analysis was also used to study the secondary structures of D-diphenylalanine nanotubes grown using PECVD. The CD spectra of nanotubes obtained under constant power and duty cycle conditions with varying frequencies from 100 Hz to 1 kHz are shown in Figure 5C. The CD spectra indicate the presence of well-pleated β-sheet structures.[34] The effect of the changing frequency on the quality of nanotubes is evident in the shown data, which was fitted using the CDPro program, and the β-sheet content was found to be ∼55% in samples obtained at lower frequency. However, in peptide nanotubes deposited at higher frequencies (>750 Hz) the unordered structure content was found to be higher, approaching about 40%. This was also confirmed through the observation of macroscopic structures via SEM, the nanotubes appeared more disorder at higher frequencies. Though the peak power and duty cycle was constant for all the depositions, the frequency of the pulse affected the morphology and characteristics of the deposited nanotubes.

Previous studies on crystallization of single amino acids in vapor phase showed that the crystal structures of the sublimates was dependent on the hydrophobic or hydrophilic nature of the side chains.[35] In particular, peptides with hydrophobic side groups such as valine and leucine have the identical crystal structure when crystallization occurred either in solution or via sublimation. Conversely, peptides with hydrophilic side groups such as phenylalanine and tyrosine have significantly different crystal structures when crystallization occurred in aqueous solutions as compared to sublimation.[35,36] Wide-angle X-ray diffraction (WAX) studies were performed on the peptide nanotubes both in grazing and in-plane incidence geometries.

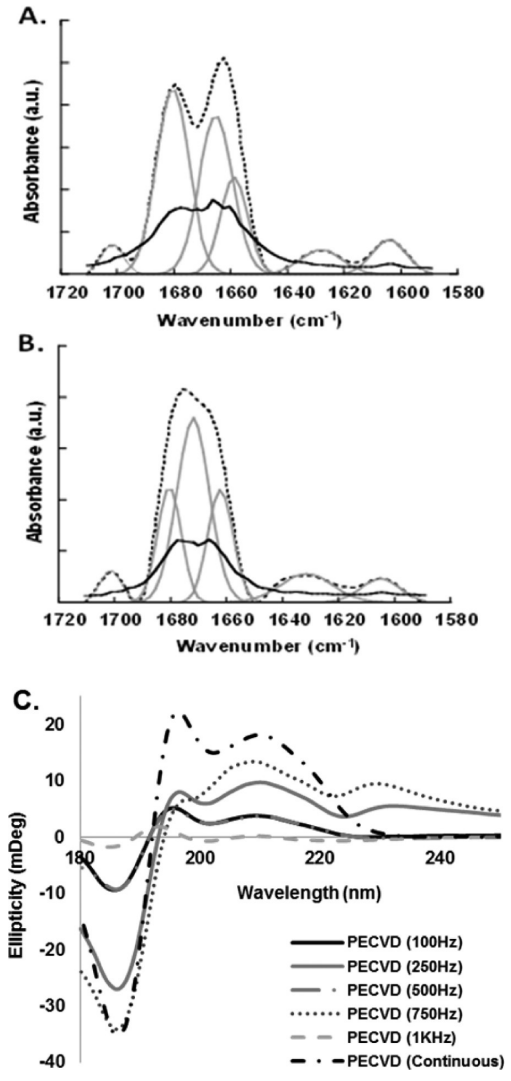

Figure 5. Deconvoluted FTIR absorbance spectrum of (A) PECVD grown D-diphenylalanine nanotubes in the amide I region indicating the β-sheet conformation; (B) PVD grown D-diphenylalanine nanotubes. The gray lines represent the individual contributions to the amide I. The dotted line represents the deduced spectra after Fourier self-deconvolution of the original spectra (black line). (C) CD spectral analysis of D-diphenylalanine nanotubes with increasing frequency grown under constant RF power of 30 W and duty cycle (25% DC).

In addition to structural information, these two methods combined also reveal the quality of the nanotube forest alignment. The results obtained are indicative of the mechanism of growth of the peptide nanotubes, showing hydrogen bonding as well as the stacking of the aromatic rings. Scans along the equator (in-plane) and meridian (out-of-plane) of a 2D GIWAX diffraction pattern demonstrate the quality of alignment (Figure 6A and inset). The diffraction peaks present along the meridian are excluded along the equator and vice versa. This was further confirmed via 1D scans in in-plane and grazing incidence geometries with a Smartlab system (Figure 6B). The quality of the alignment can be quantified via the Hermans orientation parameter S_d.[37] S_d for D-diphenylalanine nanotubes obtained from azimuthal integration of the main peak at $q = 1.24A^{-1}$ shows values greater than 0.7, indicating a highly oriented crystal arrangement (Supporting Information Figure S7). The 2D GISAX pattern for L-diphenylalanine nanotubes is identical to the one observed by Gazit et al. for PVD grown nanotubes.[15] The in-plane diffraction patterns for L-diphenylalanine and D-diphenylalanine are identical (Supporting Information Figure S8). The Hermans orientation parameter obtained from the 2D GIWAX pattern of L-diphenylalanine nanotubes is >0.8.

The observed diffraction peaks do not match the reported crystal structure of either D-diphenylalanine or L-diphenylalanine nanotubes grown from solution.[36] However, it has been previously shown that the structure of the tubes changes upon thermal treatment. The dipeptides undergo cyclization upon exposure to heat as shown in the MALDI-TOF data (Supporting Information Figure S6). Heredia et al. reported a change from a hexagonal unit cell to an orthorhombic unit cell upon heat treating their samples. We find that all diffraction peaks from the in-plane scans of D-diphenylalanine and L-diphenylalanine nanotubes in our study (Figure 6B) match the diffraction peaks observed in the previous study (Supporting Information Table S2).[38] At this stage, we do not have a complete explanation for the appearance of strong diffraction peaks observed in the out-of-plane geometry ($q = 1$ A^{-1} and 2.2 A^{-1}). Peaks with these intensities at these positions are absent with the observed unit cell. It is conceivable that the lateral packing of the tubes leads to new diffraction planes that are otherwise not seen in these samples. Further studies to verify this hypothesis are necessary.

The nanotubes composed of diphenylalanine possess high mechanical strength and stability and are stiff entities with remarkably high persistence length. The application of such nanotube arrays as thermal or electrical interface materials, as strain biosensors all depend on their mechanical properties.[39,40] The Young's modulus for individual L-diphenylalanine nanotubes of length 20−30 μm measured using contact mode AFM was estimated to be on the order of 19 GPa.[22] In this study, the peptide nanotube arrays composed of D-diphenylalanine were probed using a flat-punch indenter to measure the contact force and bulk Young's modulus. Because of the relatively dense growth of the nanotubes, the resulting arrays appear as a fibrous carpet and areas of about 40 μm were probed for the mechanical strength measurements. Multiple samples grown under similar growth conditions with an average length of about 25 μm were used for the nanoindentation tests and were probed to a depth of 20 μm, as shown in Figure 7. The diphenylalanine nanotubes were extremely stiff and undergo permanent deformation in most cases. Although, standard nanoindentation analysis cannot be applied to the PNT arrays, the force-displacement curves obtained are accurate and give sufficient data. The elastic modulus has been calculated to be in the range of 5.49 ± 0.098 GPa for D-diphenylalanine nanotubes.

■ CONCLUSION

In this study, we have deposited and characterized the peptide nanostructures composed of diphenylalanine using plasma-enhanced chemical vapor deposition. The results presented here use several microscopy techniques, mechanical testing, and spectroscopy to demonstrate that the formation of the peptide nanotubes and their different morphologies, mechanical stability, and crystalline nature are dependent on the processing conditions. Dipeptide nanotubes deposited by PECVD differ structurally from the PVD-deposited nanotubes by FTIR and X-diffraction studies. Further studies are underway to examine the structure of the dipeptide nanotubes in detail. The ability to

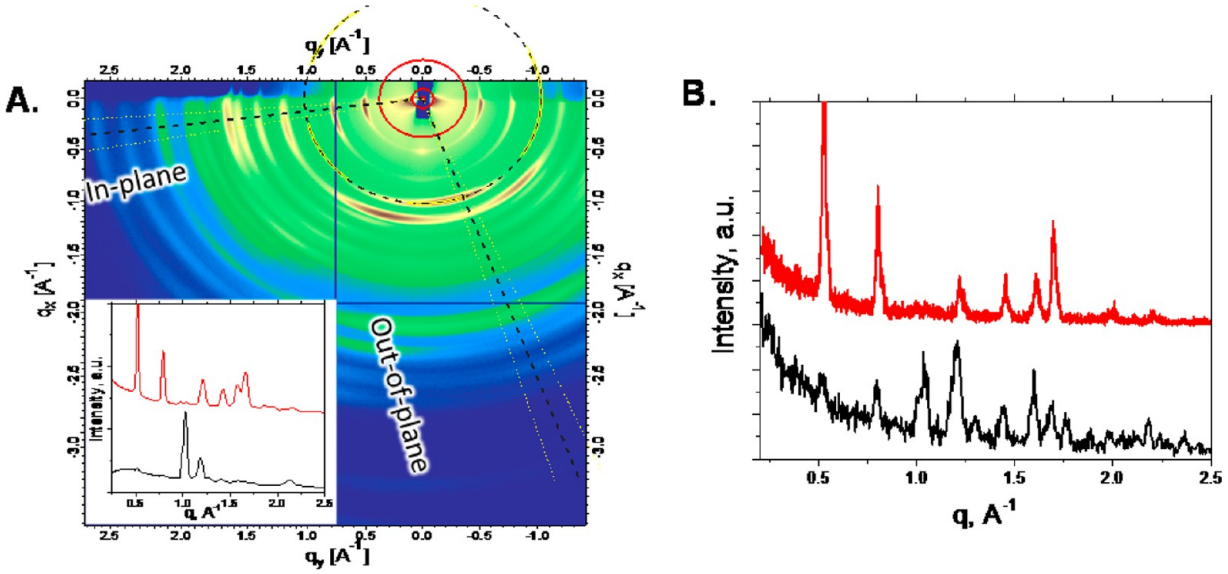

Figure 6. X-ray diffraction patterns of D-diphenylalanine nanotubes. (A) The 2D GIWAX pattern; inset: in-plane (red) and out-of-plane scans (black); (B) out-of-plane (black) and in-plane (red) 1D scans using Smartlab.

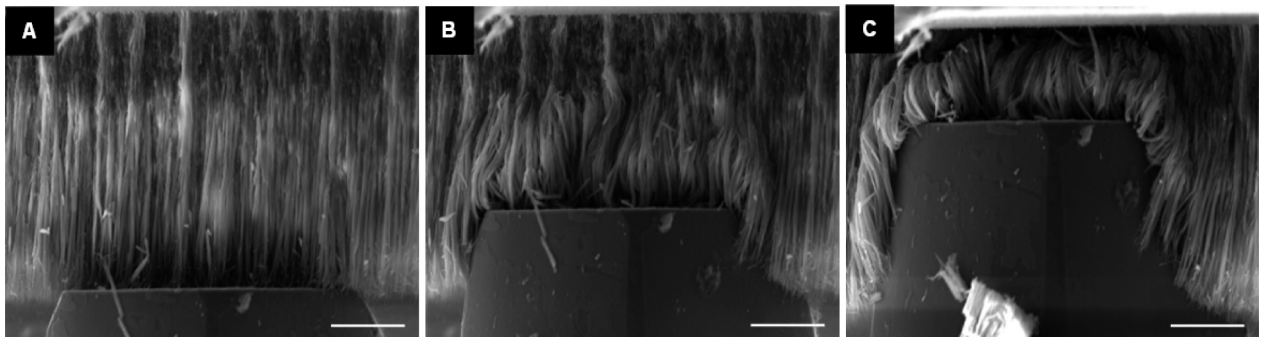

Figure 7. A flat punch indenter of 40 μm was used to compress the forest of the D-diphenylalanine nanotubes to investigate their stiffness modulus. (A) Indenter tip approaching the forest of nanotubes grown on a silicon substrate; (B) the forest of nanotubes undergoes deformation upon loading; (C) as the indenter tip moves away from the sample, the permanent deformation of the nanotubes is observed upon unloading. Scale bar in all images is 10 μm.

control deposition conditions in the PECVD process can be used to synthesize nanotubes with tunable morphologies and aspect ratios to address specific applications. The controlled phase change of the molecules allows the surfaces to be hydrophilic or hydrophobic and may lead to the use of peptide surfaces as potential biosensors for enzymes.[41] Because this fabrication technique is compatible with a variety of surfaces, it may be applicable to designing enhanced biological interfaces. Further studies of peptides with different functional groups or copolymerization with organic monomers can lead to advances in controllable electronic properties for applications in biocompatible, low-cost electronics.

■ ASSOCIATED CONTENT

Ⓢ Supporting Information

SI shows the deposition of various peptides via PECVD, the MALDI-TOF analysis data and AFM analysis in Figures S1−S9 and Tables S1−S2 have information about the FTIR analysis and XRD peaks. This material is available free of charge via the Internet at http://pubs.acs.org.

■ AUTHOR INFORMATION

Corresponding Author

*E-mail: rajesh.naik@us.af.mil. Tel: 937-255-9717.

Notes

The authors declare no competing financial interest.

■ ACKNOWLEDGMENTS

The authors acknowledge the funding support from AFOSR and AFRL. The authors thank Dr. Hao Jiang (AFRL/RX) for helpful insights into the PECVD processing conditions; Pamela Lloyd (AFRL/RX) for assistance with imaging; Dr. Kenneth Greis (University Of Cincinnati) for the MALDI-TOF analysis of peptide nanotubes; Dr. Alexander Hexemer and Dr. Eric Schaible for guidance, setup and data collection at beamline 7.3.3 at ALS/LBNL; and Dr. Robert Wheeler (AFRL/RX) for assistance in the mechanical testing studies.

■ REFERENCES

(1) Jiang, H.; O'Neill, K.; Grant, J. T.; Tullis, S.; Eyink, K.; Johnson, W. E.; Fleitz, P.; Bunning, T. J. *Chem. Mater.* **2004**, *16*, 1292−1297.
(2) Pryce Lewis, H. G.; Edell, D. J.; Gleason, K. K. *Chem. Mater.* **2000**, *12*, 3488−3494.

(3) Yang, G.; Wang, X.; Xu, Q.; Wang, S.; Tian, H.; Zheng, W. *J. Solid State Chem.* **2009**, *182*, 966−972.
(4) Friedrich, J. *Plasma Processes Polym.* **2011**, *8*, 783−802.
(5) Hayakawa, T.; Yoshinari, M.; Nemoto, K. *Biomaterials* **2004**, *25*, 119−127.
(6) Lopes, B. B.; Davanzo, C. U.; Schreiner, W.; Durrant, S. F. *Surf. Coat. Technol.* **2008**, *203*, 526−529.
(7) Jenkins, A. T. A.; Hu, J.; Wang, Y. Z.; Schiller, S.; Foerch, R.; Knoll, W. *Langmuir* **2000**, *16*, 6381−6384.
(8) Jerome Perrin, J. S.; Hollenstein, Christoph; Howling, Alan; Sansonnens, Laurent *Plasma Phys. Controlled Fusion* **2000**, *42*, B353−B363.
(9) Vasudev, M. C.; Anderson, K. D.; Bunning, T. J.; Tsukruk, V. V.; Naik, R. R. *ACS Appl. Mater. Interfaces* **2013**, *5*, 3983−3994.
(10) Aparicio, F. J.; Borras, A.; Blaszczyk-Lezak, I.; Gröning, P.; Álvarez-Herrero, A.; Fernández-Rodríguez, M.; González-Elipe, A. R.; Barranco, A. *Plasma Processes Polym.* **2009**, *6*, 17−26.
(11) Sardella, E.; Favia, P.; Gristina, R.; Nardulli, M.; d'Agostino, R. *Plasma Processes Polym.* **2006**, *3*, 456−469.
(12) Anderson, K. D.; Slocik, J. M.; McConney, M. E.; Enlow, J. O.; Jakubiak, R.; Bunning, T. J.; Naik, R. R.; Tsukruk, V. V. *Small* **2009**, *5*, 741−749.
(13) Anderson, K. D.; Young, S. L.; Jiang, H.; Jakubiak, R.; Bunning, T. J.; Naik, R. R.; Tsukruk, V. V. *Langmuir* **2012**, *28*, 1833−1845.
(14) Reches, M.; Gazit, E. *Science* **2003**, *300*, 625−627.
(15) Reches, M.; Gazit, E. *Nat. Nanotechnol.* **2006**, *1*, 195−200.
(16) Song, Y.; Challa, S. R.; Medforth, C. J.; Qiu, Y.; Watt, R. K.; Pena, D.; Miller, J. E.; Swol, F. V.; Shelnutt, J. A. *Chem. Commun.* **2004**, 1044−1045.
(17) Amdursky, N.; Molotskii, M.; Gazit, E.; Rosenman, G. *J. Am. Chem. Soc.* **2010**, *132*, 15632−15636.
(18) Adler-Abramovich, L.; Aronov, D.; Beker, P.; Yevnin, M.; Stempler, S.; Buzhansky, L.; Rosenman, G.; Gazit, E. *Nat. Nanotechnol.* **2009**, *4*, 849−854.
(19) Ryu, J.; Park, C. B. *Adv. Mater.* **2008**, *20*, 3754−3758.
(20) Ryu, J.; Park, C. B. *Chem. Mater.* **2008**, *20*, 4284−4290.
(21) Adler-Abramovich, L.; Reches, M.; Sedman, V. L.; Allen, S.; Tendler, S. J. B.; Gazit, E. *Langmuir* **2006**, *22*, 1313−1320.
(22) Kol, N.; Adler-Abramovich, L.; Barlam, D.; Shneck, R. Z.; Gazit, E.; Rousso, I. *Nano Lett.* **2005**, *5*, 1343−1346.
(23) Sedman, V. L.; Adler-Abramovich, L.; Allen, S.; Gazit, E.; Tendler, S. J. B. *J. Am. Chem. Soc.* **2006**, *128*, 6903−6908.
(24) Amdursky, N.; Molotskii, M.; Aronov, D.; Adler-Abramovich, L.; Gazit, E.; Rosenman, G. *Nano Lett.* **2009**, *9*, 3111−3115.
(25) Guo, C.; Luo, Y.; Zhou, R.; Wei, G. *ACS Nano* **2012**, *6*, 3907−3918.
(26) Enlow, J. O.; Jiang, H.; Grant, J. T.; Eyink, K.; Su, W.; Bunning, T. J. *Polymer* **2008**, *49*, 4042−4045.
(27) Harsch, A.; Calderon, J.; Timmons, R. B.; Gross, G. W. *J. Neurosci. Methods* **2000**, *98*, 135−144.
(28) Tarducci, C.; Schofield, W. C. E.; Badyal, J. P. S.; Brewer, S. A.; Willis, C. *Chem. Mater.* **2002**, *14*, 2541−2545.
(29) Maschmann, M. R.; Zhang, Q.; Wheeler, R.; Du, F.; Dai, L.; Baur, J. *ACS Appl. Mater. Interfaces* **2011**, *3*, 648−653.
(30) Yasuda, H.; Hsu, T. *J. Polym. Sci., Polym. Chem. Ed.* **1977**, *15*, 81−97.
(31) Clausen, C. H.; Jensen, J.; Castillo, J.; Dimaki, M.; Svendsen, W. E. *Nano Lett.* **2008**, *8*, 4066−4069.
(32) Ryu, J.; Park, C. B. *Angew. Chem., Int. Ed.* **2009**, *48*, 4820−4823.
(33) Haris, P. I.; Chapman, D. *Biopolymers* **1995**, *37*, 251−263.
(34) Greenfield, N. J. *Nat. Protoc.* **2007**, *1*, 2876−2890.
(35) Liu, Z.; Li, C. *Biophys. Chem.* **2008**, *138*, 115−119.
(36) Görbitz, C. H. *Chem. Commun.* **2006**, 2332−2334.
(37) Alexander, L. E. *X-Ray Diffraction Methods in Polymer Science*; Robert, E. Krieger publishing Company, 1979.
(38) Heredia, A.; Bdikin, I.; Kopyl, S.; Mishina, E.; Semin, S.; Sigov, A.; German, K.; Bystrov, V.; Gracio, J.; Kholkin, A. L. *J. Phys. D: Appl. Phys.* **2010**, *43*, 462001.
(39) Beker, P.; Rosenman, G. *J. Mater. Res.* **2010**, *25*, 1661−1666.
(40) Sopher, N. B.; Abrams, Z. R.; Reches, M.; Gazit, E.; Hanein, Y. *J. Micromech. Microeng.* **2007**, *17*, 2360.
(41) Yemini, M.; Reches, M.; Gazit, E.; Rishpon, J. *Anal. Chem.* **2005**, *77*, 5155−5159.